Philippine e-Journal for Applied Research and Development 8(2018), 34-43 ISSN 2449-3694 (Online)
http://pejard.slu.edu.ph/vol.8/2018.12.27.pdf

Effect of sintering temperature on the structure, morphology, and conductivity of LSM/YSZ composite electrode synthesized via solid state reaction

Christian C. Vaso[1,*], Arianna Benipayo[2], and Rinlee Butch Cervera[3]

[1]Department of Engineering Science, College of Engineering and Agro-Industrial Technology, University of the Philippines Los Baños; [2]Energy Storage and Conversion Materials Research Laboratory, Department of Mining, Metallurgical, and Materials Engineering, University of the Philippines Diliman
** Corresponding author (ccvaso@up.edu.ph)*

Received, 21 October 2018; Accepted, 20 December 2018; Published, 27 December 2018

Abstract

To fully achieve the advantages of hydrogen-producing solid oxide electrochemical cells (SOCs), it is necessary to synthesize electrodes that would lengthen the operating time of these SOCs. This study synthesized Lanthanum Strontium Manganite (LSM), yttria-stabilized zirconia (YSZ), and LSM/YSZ composites using the solid state reaction method. LSM/YSZ composites having 50:50 weight percent composition were sintered at two different sintering temperatures of 1150 and 1300 °C. XRD patterns showed distinct peaks of the desired phases, which can be indexed to a rhombohedral structure for LSM and to a cubic structure for YSZ. Morphological results revealed a porous composite microstructure of LSM/YSZ as compared to a more dense structure of pure LSM and pure YSZ. Upon increase in the sintering temperature, larger grain sizes and porosities were observed. The total conductivities of the samples measured at 500°C are 1.22 Scm^{-1}, 1.02 x 10^{-3} Scm^{-1} and 8.67 x 10^{-1} Scm^{-1} at activations energies of 0.20 eV, 0.85 eV and 0.22 eV for the LSM, YSZ and composite samples, respectively. These measurements were all taken under the oxygen gas environment.

Keywords: Clean fuel technology, solid oxide electrochemical cells, fuel cells, electrolysis cells

Introduction

Energy in the form of hydrogen is one of the best options for power generation through clean and sustainable means. However, to fully achieve the advantages of hydrogen-producing solid oxide electrochemical cells (SOCs), it is necessary to synthesize electrodes that would lengthen the operating time of these SOCs. SOCs include fuel cells and electrolysis cells. The mechanism of SOCs, following the basic reaction $2H_2 + O_2 \leftrightharpoons 2H_2O$, involves the use of solid oxide electrolyte to conduct ions from electrode components of the cell. Solid oxide electrolysis cell (SOEC) is just a reverse mode of operation of a solid oxide fuel cell technology. In electrolysis cells, hydrogen is produced by electrolysis of steam and such energy in the form of hydrogen can be used as fuel for power generation at any time. With this, hydrogen-producing SOECs can serve as back-up for the intermittency of renewable energy such as solar and wind energy [1, 2].

In SOEC application, electrodes such as anode and cathode play a very important role in the efficiency and performance of an electrochemical cell. Some important and target properties of the electrodes are high catalytic activity, good mixed ionic and electronic conductivity,

high mechanical and chemical stability, and good thermal coefficient of expansion which should be close to that of the solid electrolyte [3, 4]. Processing conditions such as variation of sintering temperatures can enhance some of the cell's performance and achieve high catalytic activity and conductivity. For cathode materials, for example, reports showed that different sintering temperature affects the porosity as well as the total conductivity of the cathode [4].

The anode component of SOECs must be chemically stable in highly reducing environments, and must have good ionic and electronic conductivity, suitable porosity and pore size, and relatively close thermal expansion coefficient value with electrolyte material [5, 6]. So far, the most commonly used anode materials are mixed oxides with perovskite structure like Lanthanum Strontium Manganate (LSM) because of its close thermal expansion coefficient value with yttria-stabilized zirconia or simply YSZ electrolyte. The compatibility of LSM with Y-doped Zirconia electrolyte makes it suitable electrode for electrochemical cell operations [7-9]. However, pure LSM as an anode or cathode has some drawbacks such as the formation of poor conducting compounds during cell operations [9, 11]. With this, the combination of LSM and YSZ as a composite electrode had been given attention in recent years [6-10]. It was revealed that Sr-doped $LaMnO_3$/Yttria-stabilized ZrO_2 or simply LSM/YSZ is a promising electrode material in SOEC applications. The addition of YSZ in the anode material essentially extends the electrolyte to create more triple phase boundaries (TPBs). The combination of LSM and YSZ makes the composite electrode an excellent electronic and ionic conducting electrode which has good thermal compatibility and stability [12].

The high oxygen pressures experienced by the electrode during high temperature cell operation leads to possible degradation mechanisms in triple phase boundaries (TPBs) such as chemical strains, grain boundary fracture, formation of secondary phases and delamination [13,14]. However, apparent variations in the sintering temperatures of some electrodes (i.e. LSCF-SDC, NiO/YSZ, LSCF-SDC and $Li_{10}GeP_2S_{12}$) improve some properties of the electrode such as increasing conductivity and improving the structure of the electrode [4, 15-17]. These led the researchers to check the possible effect of sintering temperature on the microstructure of composite LSM/YSZ. Studying and tailoring the sintering temperature can possibly increase the number of triple phase boundaries (TPB) where the main electrochemical reaction takes place [18]. For low porosity structure of solid oxide cells, triple phase boundaries are expected to increase because more points of interaction involving the phases of the electrode, electrolyte and oxygen take place.

This study investigates how sintering temperature (at 1150 and 1300 °C, respectively) will affect the structure, morphology, and conductivity of LSM/YSZ when synthesized using simple solid state reaction method. Conductivity measurements will also be done on different gas flow environments.

Experimental

Synthesis of LSM, YSZ and LSM/YSZ composite

The starting materials in synthesizing lanthanum strontium manganite ($La_{0.8}Sr_{0.2}MnO_3$) are La_2O_3 (99.99%, TPC), MnO_2 (99%, UNILAB Reagents), and $SrCO_3$ (99.99%, Sigma- Aldrich), while for 8 mol% YSZ ($Zr_{0.92}Y_{0.08}O_2$) are ZrO_2 (98%, High Purity Chemicals) and Y_2O_3 (99.9%, Sigma-Aldrich). The pure LSM and pure YSZ were first synthesized via solid state reactions with calcination at 1000 oC for 6h and sintering at 1200 oC for 12h. These prepared samples were then used to synthesize LSM/YSZ with 50:50 weight % composition (L50/Y50). 0.5 grams of LSM and 0.5 grams of YSZ were mixed and ground to produce 1 gram of L50Y50 composite sample. The ground samples were then oven dried, pelletized, and then sintered at 1150 °C and 1300 °C for 5h.

Characterizations

XRD analysis was run on the samples at 2 deg/min at 40 kV voltage and 30 mA current using an X-ray diffractometer Siemens Kristalloflex 760 X-ray Generator with Cu-kα tube with λ equal to 1.5406 Å. Samples were scanned at 2θ values from 3 to 90 degrees. Morphological characteristics of the samples were investigated

via scanning electron microscope using a Hitachi SU3500 SEM model coupled with Thermo Noran System 7 at 20 kV. Conductivity measurements were conducted using an electrochemical impedance spectroscopy (EIS) with a two electrode configuration. A pelletized sample is formed into a rectangular shaped pellet using a diamond saw. The two sides of the pellet were then coated with silver paste and sandwiched into two gold foils which acted as a current collector. An electrochemical workstation using BioLogic VMP-300 was utilized to conduct the measurement under oxygen and argon gas environments at temperature range of 500 °C – 700 °C. Frequency range of 5 MHz to 1 mHz was utilized during the course of the conductivity measurements.

Results and Discussion

Figure 1 shows the XRD stack patterns of the prepared samples. The peaks on Figure 1a can be indexed to a YSZ cubic structure while the peaks observed in Figure 1b can be indexed to LSM with rhombohedral structure. The calculated lattice parameters are shown in Table 1. The peaks were indexed with reference to PDF #053-0050 for LSM and PDF #030-1468 for YSZ (see Fig. 2 for the JCPDS reference XRD pattern for YSZ and LSM). The sharp peaks of YSZ in the graph evidently showed successful synthesis of the 8 mol % YSZ compound. However, small impurity peaks of yttria and monoclinic zirconia can also be observed in the XRD pattern of the as-synthesized sample. These phases are possible traces of unreacted yttria and unreacted monoclinic zirconia due to still low heat treatment temperature. In the case of the LSM samples, an impurity peak around 39 degrees is indexed to unreacted La_2O_3, which can also be attributed to the low calcination temperature used. This presence of impurity peaks in the XRD graph suggests that the calcination condition of 1000°C for 12h in solid state reaction is not enough

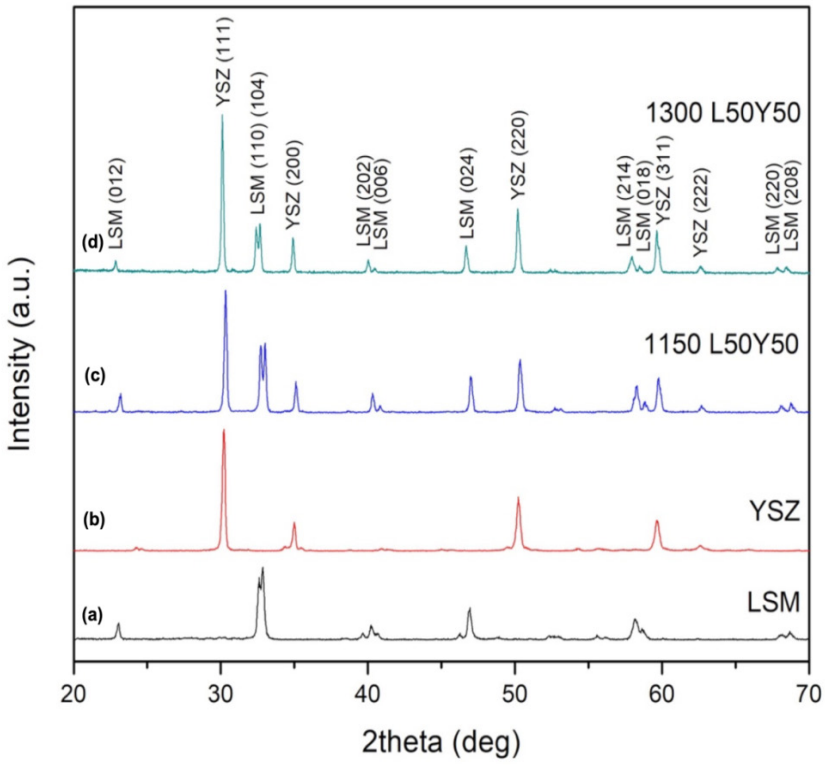

Figure 1. Stacked XRD patterns for the annealed samples. (a) LSM (calcined at 1000 °C), (b) YSZ (calcined at 1000 °C), (c) L50Y50 (sintered at 1150 °C), and (d) L50Y50 (sintered at 1300 °C)

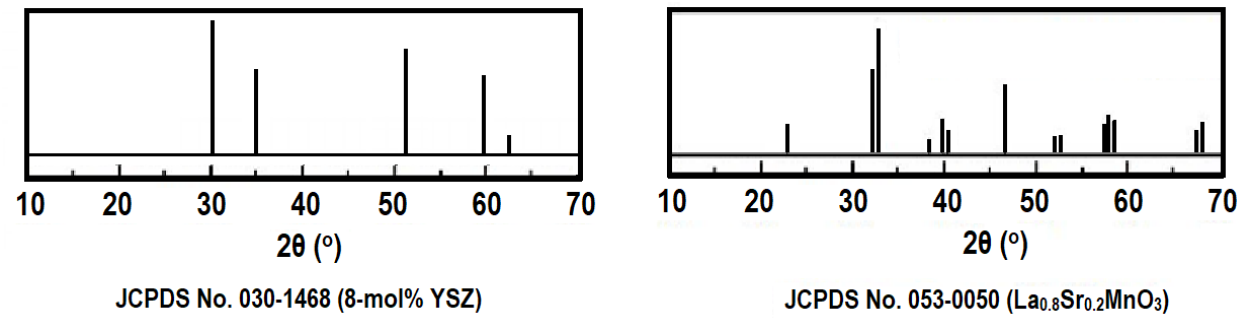

Figure 2. JCPDS references for YSZ and LSM.

to entirely allow the complete reaction of the precursor compounds. However, in the composite LSM/YSZ (Fig. 1c and 1d), the traces of the mentioned impurities were gone as shown in the XRD patterns. The XRD pattern of the composite L50Y50 shows a distinct phase of YSZ and LSM as also indexed.

The lattice parameters computed from the XRD peaks are shown in Table 1. As shown, the lattice parameters for the cubic YSZ structure is around 5.15 Å while the LSM sample have *a* and *c* lattice parameters of 3.84 Å and 7.8 Å, respectively. Also apparent on the table is the fact that the lattice parameters on the composite samples are around the values computed in their pure states.

The obtained sintered samples were also subjected to morphological characterization using SEM. The SEM images are all taken at 5000x magnification. As shown in the images in Figure 3, the YSZ particles are tiny bead-like particles with about less than 1 micrometer grain size while the LSM particles have about 2 to 4 micrometer grain size. These values are close to literature values of particle size obtained on LSM and YSZ [19]. The LSM particles appear to have beveled cube-like shape. Another important feature observed in the SEM images is the dense packing of the pure samples. Using Archimedes' principle, the relative densities of LSM and YSZ were computed to be 97.85% and 94.51%, respectively. In contrast, the composite sample shows signs of some porosity as revealed by apparent holes in their respective SEM images. For L50Y50 sintered at 1150 °C, the calculated relative density is 82.79%. The relative densities are meant to relate the theoretical densities and experimental densities of the samples. The theoretical densities are calculated based on its XRD diffraction pattern. This means that

Table 1. Calculated Lattice parameters of the samples using Rietvield refinement of Match!® Software from 20 to 70 2θ degrees.

Compound	Structure	lattice parameter	
		a, [Å]	*c*, [Å]
LSM	Rhombohedral	3.841	7.823
YSZ	Cubic	5.155	-
1150 L50/Y50	LSM: Rhombohedral	3.842	7.632
	YSZ: Cubic	5.151	-
1300 L50/Y50	LSM: Rhombohedral	5.526	13.363
	YSZ: Cubic	5.137	-

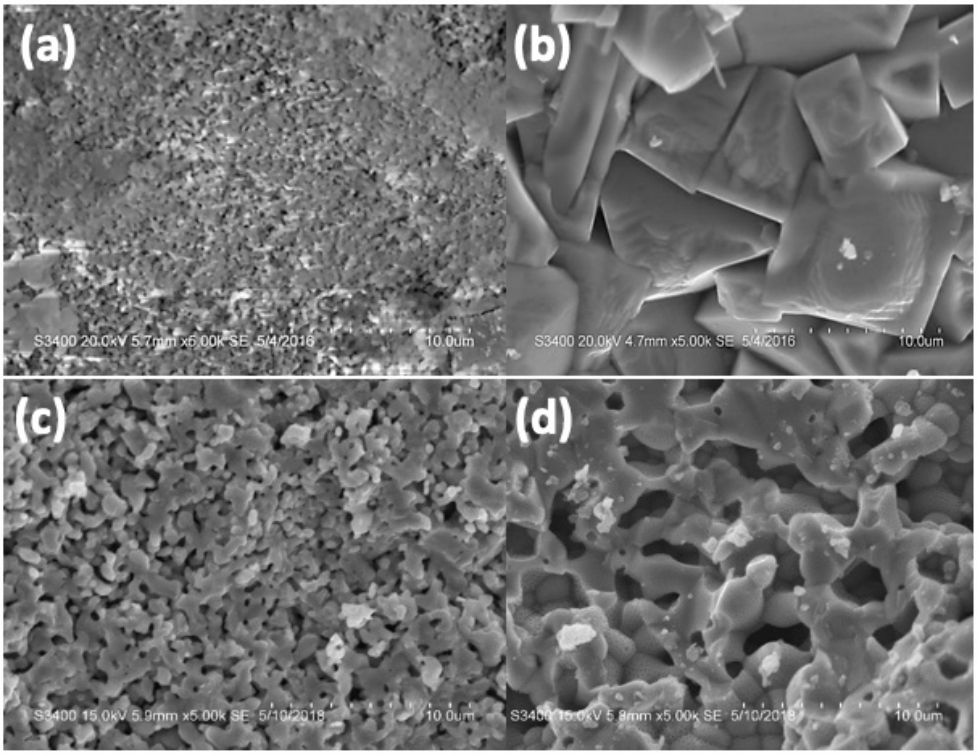

Figure 3. SEM images (a) YSZ, (b) LSM, (c) LSM/YSZ sintered at 1150 °C, (d) LSM/YSZ sintered at 1300 °C. Note that the scale bar is 1 µm per spacing.

if the sample is compact, this is its expected density. The experimental density was done via Archimedes' principle where the actual density of the synthesized sample pellet was measured. If the sample pellet has void spaces inside, it will result in lower density relative to its expected density when it is compact (theoretical density). It can also be observed that the grains are larger and agglomerated for the 1300 °C sintered LSM/YSZ. In addition, the pores become larger but lesser. For electrode material application, the 1150 °C sintered material will provide more triple-phase boundary sites with its smaller particles/grain sizes and more channels for the gas phase. The morphology of the composite sintered at 1150 °C has more porosity in it, which is the desired structure for electrode components to have more reaction sites. As it was the objective to make a more porous electrode, the sample sintered at 1150 °C is a more desirable material to be tested for its conductivity and see whether such structure will provide good performance. Thus, the conductivity of the LSM/YSZ composite sintered at 1150 °C was investigated.

Using electrochemical impedance spectroscopy, resistances were measured for all the three prepared samples under oxygen gas and argon gas flow environments and calculated for their conductivity. Figures 4-6 show the Arrhenius type plots of the conductivity [20] for YSZ, LSM, and LSM/YSZ, respectively. For electrodes materials, either cathode or anode in an electrochemical device like solid oxide cells, it should have mixed conductivity, electronic and ionic conductivity. Electronic conductivity is the conduction of electrons while ionic conductivity is the oxide ion conduction. In this study, the material that conducts oxide ion is YSZ while LSM is for the electrons. Such high ionic and electronic conductivity is necessary for a good cell performance of the device. In all the graphs, the conductivity values under argon gas condition are lower as compared to conductivities of the three samples under oxygen gas flow environment.

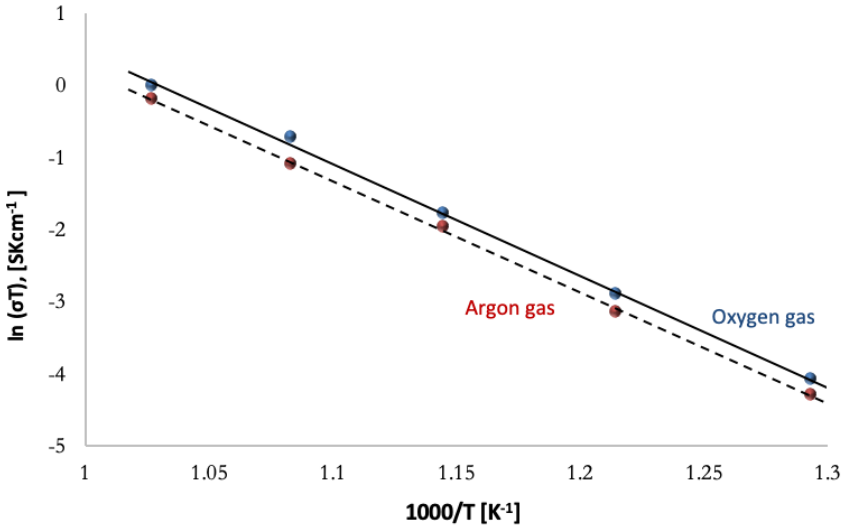

Figure 4. Arrhenius plot of YSZ conductivity under Argon and Oxygen gas environments at intermediate temperature range from 773.15 K to 973.15 K.

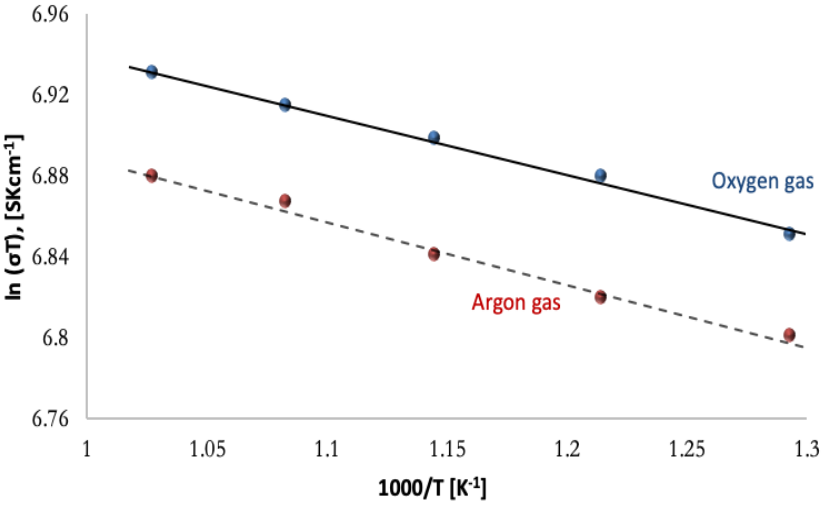

Figure 5. Arrhenius plot of LSM conductivity under Argon and Oxygen gas environments at intermediate temperature range from 773.15 K to 973.15 K.

Table 2. Summary of activation energies computed from the samples

Compound	Activation energy [eV]	
	O_2 Environment	*Ar Environment*
YSZ	0.85	0.84
LSM	0.16	0.17
L50/Y50	0.22	0.22

Figure 4 shows the temperature dependence of the YSZ sample's conductivity while Table 2 displays the corresponding activation energies. The R^2 of both lines, which is around 99 %, fits well with the plotted conductivities versus temperature. The conductivity of YSZ increases with temperature, both in the argon and oxygen gas flow environments. The highest conductivity for this sample is 1.02 x 10^{-3} Scm^{-1}, measured at 973.15 K. YSZ is known to have good ionic conductivity but very low electronic conductivity [10]. Thus, the conductivity of YSZ in this experiment can be attributed to the ionic diffusion throughout the sample pellet. This is further backed up by the activation energy computed in the samples under oxygen and argon gas. The activation energy calculated is around 0.8 eV, which falls within the typical activation energy for oxide ion conductivity in this YSZ solid electrolyte [21].

With regard to the conductivity of LSM with temperature, Figure 5 displays the Arrhenius type plot of the conductivity for LSM. As shown in the figure, the conductivity of LSM under oxygen gas is generally higher at varying temperatures as compared to its conductivity under argon gas environment. The oxidizing atmosphere may have an effect on the defects in LSM such as increase in the manganese oxidation state (Mn^{3+} and Mn^{4+}) and oxygen vacancies [22] that affect the total conductivity as observed in our study. However, further study is needed to investigate thoroughly the effect of oxygen partial pressure environment on LSM structure and its conductivity. The activation energy calculated in both atmospheres is about 0.2 eV as shown in Table 2. This suggests that the governing conductivity is highly electronic. The highest conductivity value for LSM under oxygen gas is 1.22 Scm^{-1}, measured at 773.15 K. The Arrhenius plot of the composite sample of LSM/YSZ also depicted the same behavior, as shown in Figure 6. Lower conductivity values are observed on the argon gas flow environment. The activation energies in both gas environments are almost the same at about 0.22 eV.

Figure 7 shows the conductivity behavior of the three samples in one Arrhenius-type plot. It can be observed that pure YSZ has lower total conductivity as compared to LSM and LSM/YSZ composite and has higher activation energy. For LSM and LSM/YSZ, the plot revealed an almost comparable conductivity, which suggests that the sample's total conductivity is mainly governed by the high electronic conductivity coming from LSM as supported by the calculated low activation energy. For conductivity measurements under oxygen gas flow environment, LSM has 1.22

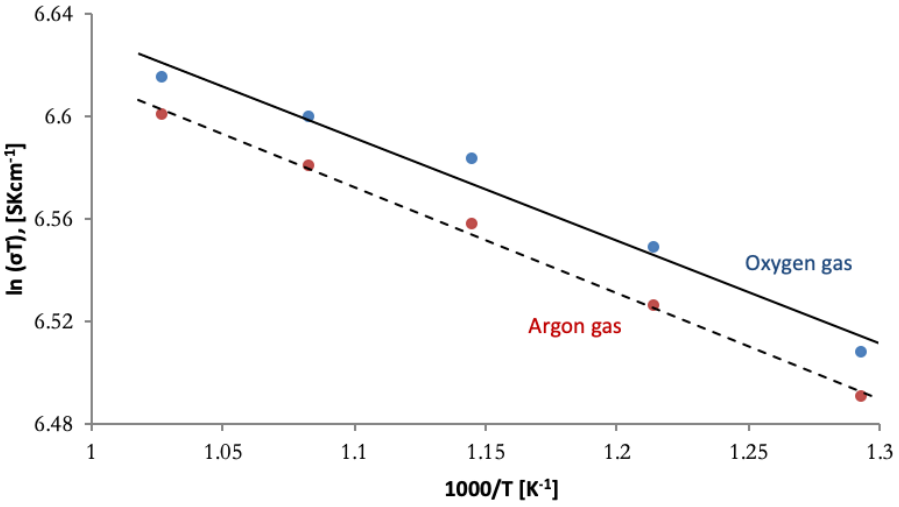

Figure 6. Arrhenius plot for 1150 L50Y50 under Argon and Oxygen gas environments at intermediate temperature range from 773.15 K to 973.15 K.

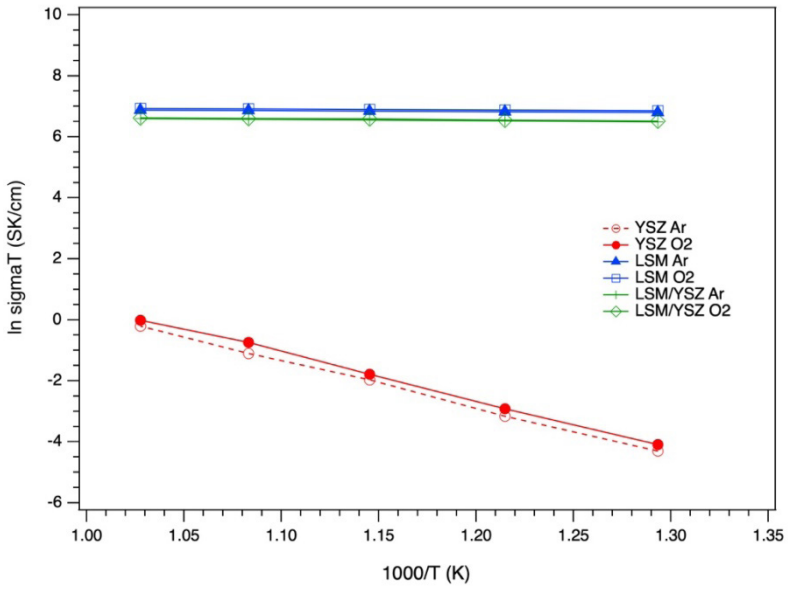

Figure 7. Arrhenius-type plot of the total conductivities of pure YSZ, pure LSM, and 1150 LSM/YSZ under Ar and O_2 gas flow environment from 500 to 700 °C.

Scm^{-1} while YSZ has 1.02 x 10^{-3} Scm^{-1} at 500 °C with activation energies of 0.85 eV and 0.16 eV, respectively. Meanwhile, the calculated conductivity of LSM/YSZ composite sample is about 8.67 x 10^{-1} Scm^{-1} at 500 °C with an activation energy of 0.22 eV.

Conclusion

The synthesis of LSM, YSZ and LSM/YSZ via solid state reaction technique was successfully conducted. The XRD patterns showed the formation of rhombohedral LSM and cubic YSZ structure. As observed from morphological analysis, increasing the sintering temperature from 1150 to 1300 °C led to grain growth and resulted in lesser porosities. From this, the 1150 °C obtained sample is desirable in terms of more triple boundary reaction sites due to less agglomeration and more porous structure. Conductivity measurements of this LSM/YSZ composite revealed high total conductivity, which is mainly contributed by the electronic conduction coming from LSM.

Acknowledgments

This study was financially supported by the Philippine-California Advanced Research Institute – Commission on Higher Education (PCARI-CHED) Institute for Information Infrastructure Development GREENPower research grant (IIID-2015-09) and in part by the Engineering Research and Development for Technology scholarship under the Department of Science and Technology (ERDT-DOST).

References

[1] F. Suleman, I. Dincer, and M. Agelin-Chab. (2015). "Environmental impact assessment and comparison of some hydrogen production options." International Journal of Hydrogen Energy, 40(21), 6976-6987. DOI 10.1016/j.ijhydene.2015.03.123

[2] P. Kazempoor and R.J. Braun. (2015). "Hydrogen and synthetic fuel production using high temperature solid oxide electrolysis cells (SOECs)." International Journal of Hydrogen Energy, 40(9), 3599-

3612. DOI 10.1016/j.ijhydene.2014.12.126

[3] A. Brisse and P. Mocoteguy. (2013). "A review and comprehensive analysis of degradation mechanisms of solid oxide electrolysis cells." International Journal of Hydrogen Energy, 38, 15887-15902. DOI 10.1016/j.ijhydene.2013.09.045

[4] F. Bueta, J.F. Imperial and R.B. Cervera. (2017). "Structure and conductivity of NiO/YSZ composite prepared via modified glycine-nitrate process at varying temperature." Ceramics International, 43 (18), 16174-16177. DOI 10.1016/j.ceramint.2017.08.193

[5] M. Ni, Michael K.H. Leung, D. Leung. (2008). "Technological development of hydrogen production by Solid Oxide electrolyzer cell (SOEC)." International Journal of Hydrogen Energy, 33(9), 2337-2354. DOI 10.1016/j.ijhydene.2008.02.048

[6] R.A. Avila, T. Tambago, R.B. Cervera. (2018). "Preparation of porous LSM/YSZ composite with varying grain size of YSZ precursor using solid state reaction method." Materials Science Forum 9(17), 93-97. DOI 10.4028/www.scientific.net/MSF.917.93

[7] H. A. Taroco, J.A.F. Santos, R.Z. Domingues, T. Matencio. (2011). "Ceramic materials for solid oxide fuel cells." Advances in Ceramics, Costas Sikalidis, IntechOpen. DOI: 10.5772/18297.

[8] F. Bidrawn, J.M. Vohns, and R.J. Gorte. (2010). "Fabrication of LSM–YSZ composite electrodes by electrodeposition." Journal of the Electrochemical Society, 157(11), B1629-B1633. DOI 10.1149/1.3484096

[9] C.A. Cortes-Escobedo, F. S. De Jesus, G. T. Villaseñor, J.M. Saldaña, A.M. Blarin-Miro. (2012). "Characterization of ceramic materials synthesized by mechanosynthesis for energy applications." Scanning Electron Microscope, Viacheslav Kazmiruk, IntechOpen. DOI 10.5772/35583.

[10] M. Liang, B. Yu, M. Wen, J. Chen. (2009). "Preparation of LSM–YSZ composite powder for anode of solid oxide electrolysis cell and its activation mechanism." Journal of Power Sources, 190(2), 341-345. DOI 10.1016/j.jpowsour.2008.12.132.

[11] N. Li, M. Keane, M. Mahapatra, P. Singh. (2013). "Mitigation of the delamination of LSM anode in solide oxide electrolysis cells using manganese-modified YSZ." International Journal of Hydrogen Materials, 38(15), 2698-6303. DOI 10.1016/j.ijhydene.2013.03.036.

[12] A. Tarancón. (2009). "Strategies for lowering solid oxide fuel cells operating temperature." Energies, 2(4), 1130-1150. DOI 10.3390/en20401130

[13] M. Keane. (2014). "Materials interactions and degradation processes in solid oxide electrolysis cells." PhD Thesis. University of Connecticut.

[14] A. Nechache, M. Cassir, A. Ringuede. (2014). "Solid Oxide electrolysis cell analysis by means of electrochemical impedance spectroscopy: A review." Journal of Power Sources, 258. 164-181. DOI 10.1016/j.jpowsour.2014.01.110.

[15] F. Yi, S. Song, W. Wu, Z. Yan, D. Yuan, C. Fu, J. Shi, X. Zhang, Y. Xiang. (2018). "Effects of sintering temperatures on the crystallinity and electrochemical properties of the $Li_{10}GeP_2S_{12}$ via solid state sintering method." Material Science and Engineering, 394. DOI 10.1088/1757-899X/394/2/022038.

[16] NA. Baharuddin, A. Muchtar, MR. Somalu, M. Ali, H. Rahman. (2016). "Influence of sintering temperature on the polarization resistance of $La_{0.6}Sr_{0.4}Co_{0.2}Fe_{0.8}O_{3-\delta}$ – SDC carbonate composite cathode." Ceramics-Silikaty, 60(2), 114-121. DOI 10.13168/cs.2016.0017.

[17] Y. Guan, X. Pan, G. Liu, Z. Liang. (2013). "Analysis of impact of sintering temperature on microstructure of LSCF-SDC composite cathodes using nano-CT." The international Society of Optical Engineering, 8851. DOI 10.1117/12.2026149.

[18] X. Lu, T. Heenan, J. Bailey, T. Li, K. Li, D. Brett, P. Shearing. (2017). "Correlation between triple phase boundary and the microstructure of solid oxide fuel cell anodes: The role of composition, porosity and Ni densification." Journal of Power Sources, 365, 210-219. DOI 10.1016/j.jpowsour.2017.08.095.

[19] K-S. Sim, K-K Bae, C-H Kim, K-B Park. (2006). "Electrochemical performances

of LSM/YSZ composite electrode for high temperature steam electrolysis," Korea Institute of Energy Research. WHEC 16, 13-16.

[20] R.B. Cervera, Y. Oyama, I Oikawa, H. Takamura, S. Yamaguchi. (2014). "Nanograined Sc-doped BaZrO3 as a proton conducting solid electrolyte for intermediate temperature solid oxide fuel cells (IT-SOFCs)." Solid State Ionics, 264, 1-6.

[21] M.B. Villanueva, R.M. Garcia, R.B. Cervera. (2018). "Synthesis and characterization of SC and Y co-doped zirconia (Zr0.84Y0.08Sc0.08O1.92) electrolyte prepared by sol-gel method." International Journal of Materials Science and Engineering, 6(4), 99-105.

[22] S. Tanasescu, C. Marinescu, F. Maxim, A.Sofornia, N. Totir. (2011). "Evaluation of manganese and oxygen content in $La_{0.7}Sr_{0.3}MnO_{3-\delta}$ and correlation with the thermodynamic data." Journal of Solid State Electrochemistry, 15, 189-196.